

A Physics-informed Machine Learning-based Control Method for Nonlinear Dynamic Systems with Highly Noisy Measurements

Mason Ma^a, Jiajie Wu^a, Chase Post^a, Tony Shi^a, Jingang Yi^b, Tony Schmitz^{c,d}, and Hong Wang^d

^a*Department of Industrial and Systems Engineering, University of Tennessee Knoxville, Knoxville, TN 37996*

^b*Department of Mechanical and Aerospace Engineering, Rutgers University, Piscataway, NJ 08854*

^c*Department of Mechanical, Aerospace, and Biomedical Engineering, University of Tennessee Knoxville, Knoxville, TN 37996*

^d*Oak Ridge National Laboratory, Oak Ridge, TN 37831*

Abstract

This study presents a physics-informed machine learning-based control method for nonlinear dynamic systems with highly noisy measurements. Existing data-driven control methods that use machine learning for system identification cannot effectively cope with highly noisy measurements, resulting in unstable control performance. To address this challenge, the present study extends current physics-informed machine learning capabilities for modeling nonlinear dynamics with control and integrates them into a model predictive control framework. To demonstrate the capability of the proposed method we test and validate with two noisy nonlinear dynamic systems: the chaotic Lorenz 3 system, and turning machine tool. Analysis of the results illustrate that the proposed method outperforms state-of-the-art benchmarks as measured by both modeling accuracy and control performance for nonlinear dynamic systems under high-noise conditions.

Keywords: data-driven modeling and control, nonlinear dynamics, physics-informed machine learning, system identification, discrete optimization, model predictive control

1. Introduction

The field of dynamic systems and control fundamentally revolves around determining the inputs for altering, directing, and optimizing complex system outputs in some desired manners. Effective controller design techniques, like optimal control [1] and model predictive control (MPC) [2], rely heavily on accurate system modeling, especially for nonlinear dynamics with noisy measurements. In contrast to physical model-based control methods, data-driven modeling-based control methods have become increasingly relevant alongside advances in metrology, data science, machine learning and artificial intelligence.

There are a wide variety of data-driven modeling techniques amenable for controller design [3]. Autoregressive modeling is often considered to be the simplest technique [4]. Many types of autoregressive models exist, which include linear and nonlinear models like ARX, ARMA, NARX, and NARMAX [5]. In addition, subspace identification methods (SIM) build linear state space models via analysis of the spanned space of rows and columns of matrices created from time series input-output data [6-8]. Linear approximation models of nonlinear dynamics can be constructed by dynamic mode decomposition (DMD) using time series data and singular value decomposition [9, 10]. Previous work has shown DMD to produce modes that are approximations of the modes of Koopman operators [11-13]. Moreover, other methods such as kernel-based Gaussian processes (GP) [14-17] and neural networks (NN) [5, 18] have been used to model dynamic systems. The aforementioned methods have been combined with existing control techniques to deal with modeling and control issues for dynamic systems of a variety of scales and scopes [15, 19]. However, these data-driven modeling techniques, whether they produce input-output or state-space models, are often black-box. In other words, they lack interpretability of physical meaning, generalization to new data, and robustness to noisy measurements as compared to accurate physical models. Addressing these limitations is a prerequisite for identifying physical models from data using physics-informed machine learning methods.

Recent advances in data-driven modeling and control by physics-informed machine learning mainly adopt symbolic regression and linear regression with sparsity to obtain white-box (physical) models. The representative method, SINDY-MPC [20], is able to learn accurate physical models from very few examples in time, making it considerably more data efficient than neural networks for MPC, but with comparable or superior control performance, when the systems are symbolically representable [3]. The main procedures of SINDY-MPC are as follows: predefine a nonlinear set of state and control variables, obtain a white-box system model from data via sparse linear regression with a threshold sequential least squares algorithm, then integrate the MPC for model-based control. However, a caveat is the heuristic of threshold sequential least squares algorithm used by SINDY-MPC. By implication, this means SINDY-MPC cannot accurately obtain system models under noisy conditions and therefore results in unstable control performance. More recently, discrete optimization related techniques as exact methods have been developed for solving sparse linear regression for data-driven modeling of nonlinear dynamic systems [21, 22]. Results in [21] demonstrated that discrete optimization-based machine learning methods can obtain the governing equations of dynamic systems from highly noisy data without control input.

In the current study, we present a physics-informed machine learning-based control (PIMLC) method developed for the purpose of handling nonlinear dynamic systems with highly noisy measurements. This is done by first extending current discrete optimization-based machine learning capabilities to learn white-

box models of nonlinear dynamics with control, and then integrating the acquired models into the MPC framework for control applications. Simulation experiments on the chaotic Lorenz 3 system and turning machine tool are conducted with performance comparisons to the state-of-the-art benchmarks for both modeling and control. The primary contributions of this work are as follows.

- The PIMLC method can acquire more accurate white-box models for nonlinear dynamics with control under high-noise conditions compared to SINDY-MPC. This contention is made because discrete optimization based exact method can solve the resulting sparse linear regression problem to optimality, despite highly noisy data. PIMLC significantly outperforms the heuristic threshold sequential least squares algorithm used by SINDY-MPC. This is evidenced by the simulation experiments of the chaotic Lorenz 3 system and turning machine tool. In specific, the anti-noise capacity of PIMLC is at least 10 times and 100 times better than SINDY-MPC, respectively.
- The PIMLC method can achieve superior data-driven model-based control performance. Benefiting from the accuracy and robustness of the white-box models acquired from highly noisy data, the control system performance of PIMLC significantly outperforms SINDY-MPC and NN-based MPC (NARX-MPC). For constant set point and trajectory tracking control settings of the chaotic Lorenz 3 system, the steady state errors of PIMLC are several orders of magnitude lower than SINDY-MPC and are less than 69% of the steady state errors of NARX-MPC.
- Finally, PIMLC can be used for pre-process selection of stable cutting parameters with maximized material removal rate in turning machine tool operations. To our best knowledge, this is the first optimal control formulation for cutting parameter selection of turning dynamics. The optimization accuracy and solution time using MPC in PIMLC is superior to the accuracy and time used by traditional sampling-based enumeration algorithm used in time domain simulation analysis. Moreover, results from this study provide evidence for the application potential of PIMLC for milling machine tools to suppress chatter in real-world settings.

The rest of this paper is organized as follows. The problem statement is presented in Section 2. The proposed PIMLC method is described in Section 3. The case study results of the proposed PIMLC method on two testbeds are presented in Section 4. Section 5 concludes this paper.

2. Problem Statement of Data-Driven Control

We consider the problem of data-driven modeling-based control of dynamic systems of the form

$$\dot{\mathbf{x}} = \mathbf{f}(\mathbf{x}(t), \mathbf{u}(t), \mathbf{w}(t)), \quad (1)$$

$$\mathbf{y} = \mathbf{g}(\mathbf{x}(t), \mathbf{u}(t), \mathbf{v}(t)), \quad (2)$$

where $\mathbf{x}(t) = [x_1(t), \dots, x_J(t)] \in \mathbb{R}^{1 \times J}$ denotes the vector of J state variables of the system at time t , vector $\mathbf{y}(t) = [y_1(t), \dots, y_M(t)] \in \mathbb{R}^{1 \times M}$ represents all the measurable output variables of the system, and vector $\mathbf{u}(t) = [u_1(t), \dots, u_S(t)] \in \mathbb{R}^{1 \times S}$ is the vector of input/control variables to the system. Vector $\mathbf{w}(t) \in \mathbb{R}^{1 \times J}$ is the exogenous disturbances to the state variables, and vector $\mathbf{v}(t) \in \mathbb{R}^{1 \times M}$ is the noise imposed on the output measurements. In this paper, we assume full state measurement and $\mathbf{g}(\cdot)$ is thus known. In addition, disturbances $\mathbf{w}(t)$ and $\mathbf{v}(t)$ are assumed to be included in the measurements of \mathbf{x} and can be omitted in the following. $\mathbf{f}(\mathbf{x}(t), \mathbf{u}(t))$ are generally nonlinear functions representing the unknown right-hand-sides of the governing equations of the dynamic system that need be discovered from the data. For the cases where discrete-time dynamic systems are used, the dynamic systems considered are of the form

$$\mathbf{x}_{k+1} = \mathbf{F}(\mathbf{x}_k, \mathbf{u}_k, \mathbf{w}_k), \quad (3)$$

$$\mathbf{y}_{k+1} = \mathbf{G}(\mathbf{x}_k, \mathbf{u}_k, \mathbf{v}_k), \quad (4)$$

where k is the discrete time index. Functions $\mathbf{F}(\cdot)$ and $\mathbf{G}(\cdot)$ are the discrete-time dynamic system equations of $\mathbf{f}(\cdot)$ and $\mathbf{g}(\cdot)$, respectively, which can be obtained using numerical discretization techniques like, for example, the forward Euler method. In the following, we use the notations of continuous-time dynamic systems unless otherwise stated. The problem of interest is to both identify the unknown nonlinear dynamics $\mathbf{f}(\cdot)$ and determine the control inputs \mathbf{u} such that the dynamic system performs satisfactorily. Mathematically, the ultimate goal is to design a controller

$$\mathbf{u}(t) = \pi(\mathbf{y}(t), \mathbf{r}(t)), \quad (5)$$

that optimizes a cost function

$$L := \int_{t_0}^{t_f} \ell(\mathbf{x}(t), \mathbf{r}(t)) dt, \quad (6)$$

where $\mathbf{r}(t) \in \mathbb{R}^{1 \times J}$ is a reference trajectory for the state variables to track within the closed-loop feedback control system, and $\pi(\cdot)$ is the control policy function. The cost function L is defined as the integral of $\ell(\cdot)$ within the period $[t_0, t_f]$ of interests, where the latter is usually problem dependent. In general, the controller $\mathbf{u}(t)$ is also a dynamic system, which relies heavily on the identification of $\mathbf{f}(\cdot)$ and the optimization techniques placed upon L .

As for the data, the in-process measurements provide both system output data and control signals. According to our assumption of full state measurement of the dynamic system, the measurements of \mathbf{x} are given as time series data with series length N in the matrix form $\mathbf{X} \in \mathbb{R}^{N \times J}$. The time derivative matrix $\dot{\mathbf{X}} \in \mathbb{R}^{N \times J}$ can be either numerically calculated or directly measured. The time series data of inputs \mathbf{u} is measured as $\mathbf{U} \in \mathbb{R}^{N \times S}$. Note matrix \mathbf{U} is used for system identification by regulating particular inputs, such as impulse, step, and sinusoidal functions. The measurements \mathbf{X} and/or $\dot{\mathbf{X}}$ are taken upon noise contamination under which system identification and subsequent control of the dynamic system can be challenging.

3. Proposed Physics-informed Machine Learning-based Control Method

This section presents the proposed PIMLC method. PIMLC consists of two components: first, identification of the dynamic system model using a discrete optimization-enabled physics-informed machine learning algorithm, and second application of the established model predictive control techniques. The latter is done by using the acquired model to enable enhanced data-driven control.

Fig. 1 shows the schematic illustration of PIMLC for data-driven control of the studied dynamic systems. The time series data \mathbf{x} and \mathbf{u} is fully utilized by the physics-informed machine learning algorithm to obtain the model $\hat{\mathbf{f}}(\mathbf{x}, \mathbf{u})$. Then, the best control decision \mathbf{u}_{p+1}^* in the next step will be acquired via model predictive control using the acquired model.

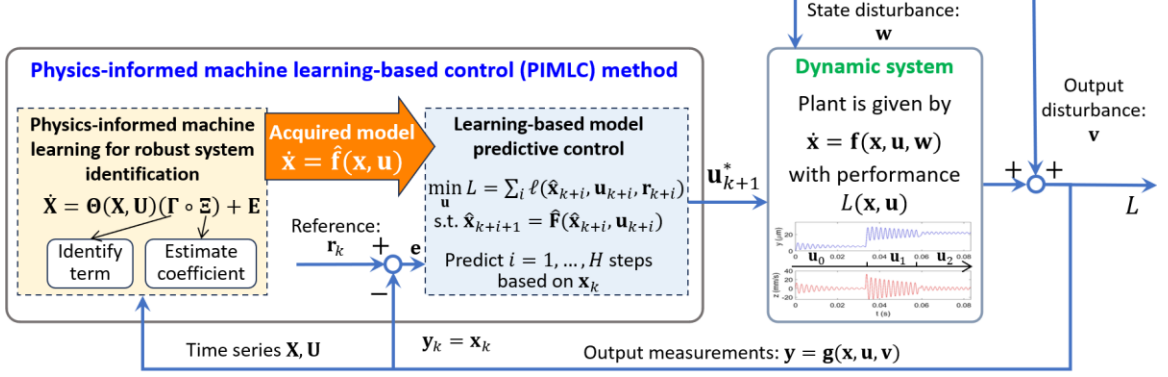


Fig. 1. Schematic illustration of the proposed physics-informed machine learning-based control (PIMLC) method

3.1 Physics-informed machine learning for robust system identification

Here we extend the discrete optimization-based physics-informed machine learning algorithm [21] to include both the state and control variables for robust system identification. The main idea behind system identification of unknown nonlinear dynamics $\mathbf{f}(\cdot)$ using discrete optimization is to identify the functional terms and the associated coefficients in a separate manner. The proposed algorithm learns the unknown dynamic system model from time series measurements, grounded in the fact that the right-hand-side of the governing equations of most dynamic systems include relatively few terms. Thus, discrete optimization-based physics-informed machine learning can be effective in explicitly controlling the sparsity of terms in $\mathbf{f}(\mathbf{x}, \mathbf{u})$, resulting in parsimonious models.

To do so, a dictionary of basis functions $\boldsymbol{\theta}(\mathbf{x}, \mathbf{u})$ consisting of P candidate terms for $\mathbf{f}(\mathbf{x}, \mathbf{u})$ is first constructed by basis expansion of \mathbf{x} and \mathbf{u} , denoted by

$$\boldsymbol{\theta}(\mathbf{x}, \mathbf{u}) = [\theta_1(\mathbf{x}, \mathbf{u}) \ \theta_2(\mathbf{x}, \mathbf{u}) \ \cdots \ \theta_P(\mathbf{x}, \mathbf{u})], \quad (7)$$

where $\theta_1(\mathbf{x}, \mathbf{u}), \dots, \theta_P(\mathbf{x}, \mathbf{u})$ denote the linear or nonlinear operators of elements in \mathbf{x} and/or \mathbf{u} . For brevity, we denote θ_p as the p -th term of $\boldsymbol{\theta}(\mathbf{x}, \mathbf{u}) \in \mathbb{R}^{1 \times P}$ in the following. For example, $\boldsymbol{\theta}(\mathbf{x}, \mathbf{u})$ can be constructed to include the constant, polynomial, trigonometric terms, etc., of \mathbf{x} and/or \mathbf{u} , that is

$$\boldsymbol{\theta}(\mathbf{x}, \mathbf{u}) = [1 \ \mathbf{x} \ \mathbf{u} \ (\mathbf{x} \otimes \mathbf{u}) \ (\mathbf{x} \otimes \mathbf{x}) \ \cdots \ \sin(\mathbf{x}) \ \sin(\mathbf{u}) \ \cdots], \quad (8)$$

where $\mathbf{x} \otimes \mathbf{u}$ denotes the vector of the element-wise products of \mathbf{x} and \mathbf{u} . It is remarked that the

construction of $\boldsymbol{\theta}(\mathbf{x}, \mathbf{u})$ should incorporate physical knowledge of the studied system to ensure that all terms of $\mathbf{f}(\mathbf{x}, \mathbf{u})$ are included in $\boldsymbol{\theta}(\mathbf{x}, \mathbf{u})$. During this procedure, human interaction is critical in determining the initial pool of candidate terms in $\mathbf{f}(\mathbf{x}, \mathbf{u})$. The initial pool of candidate terms usually consists of polynomials. By considering the underlying physical knowledge of the studied systems, the addition or removal of terms in $\boldsymbol{\theta}(\mathbf{x}, \mathbf{u})$ is performed. For example, trigonometric terms seem to be common and necessary for modelling mechanical systems. The design of features is thus an iterative process with frequent interactions between machine learning and humans. In this work, we assume that the unknown functions of $\mathbf{f}(\mathbf{x}, \mathbf{u})$ live in the functional space spanned by $\boldsymbol{\theta}(\mathbf{x}, \mathbf{u})$. Mathematically, we have

$$\mathbf{f}(\mathbf{x}, \mathbf{u}) = \boldsymbol{\theta}(\mathbf{x}, \mathbf{u}) \cdot \boldsymbol{\Xi}, \quad (9)$$

where $\boldsymbol{\Xi} = [\boldsymbol{\xi}_1 \ \boldsymbol{\xi}_2 \ \cdots \ \boldsymbol{\xi}_J] \in \mathbb{R}^{P \times J}$ is the matrix of coefficients, and each column $\boldsymbol{\xi}_j \in \mathbb{R}^{P \times 1}$ refers to those for function $f_j(\mathbf{x}, \mathbf{u})$, $j \in \mathcal{J}$, where throughout this paper, we define set $\mathcal{J} = \{1, 2, \dots, J\}$.

To discover the unknown $\mathbf{f}(\mathbf{x}, \mathbf{u})$ is to obtain the coefficients $\boldsymbol{\Xi}$. Note that the identification of the governing equation is independent for each $x_j(t)$. We use $f_j(\mathbf{x}, \mathbf{u})$ as an example. We denote the j -th column of $\dot{\mathbf{X}}$ as $\dot{\mathbf{x}}_j$. Instead of controlling sparsity through regularization on $\boldsymbol{\xi}_j$ for $\forall j \in \mathcal{J}$, we aim to directly control the number of active terms in $\boldsymbol{\xi}_j$, denoted by κ_j and $\kappa_j \in \mathcal{P} := \{1, \dots, P\}$, then identify the optimal combination of terms by discrete optimization. To begin with, we define an indicator matrix $\boldsymbol{\Gamma} \in \mathbb{B}^{P \times 1}$ to denote the existence of θ_p in $f_j(\mathbf{x}, \mathbf{u})$ for $j \in \mathcal{J}$:

$$\boldsymbol{\Gamma} := [\boldsymbol{\gamma}_1 \ \boldsymbol{\gamma}_2 \ \cdots \ \boldsymbol{\gamma}_J], \quad (10)$$

where $\boldsymbol{\gamma}_j = (\gamma_{1j} \ \cdots \ \gamma_{pj})^T \in \mathbb{B}^{P \times 1}$ and \mathbb{B} is the Boolean domain $\mathbb{B} = \{0, 1\}$, i.e.,

$$\gamma_{pj} = \begin{cases} 1, & \text{if } f_j(\mathbf{x}, \mathbf{u}) \text{ includes } \theta_p, \\ 0, & \text{otherwise.} \end{cases} \quad (11)$$

With the noisy time series measurements \mathbf{X} and \mathbf{U} , Eq. (9) can be further written as

$$\dot{\mathbf{X}} = \boldsymbol{\Theta}(\mathbf{X}, \mathbf{U})(\boldsymbol{\Gamma} \circ \boldsymbol{\Xi}) + \mathbf{E}, \quad (12)$$

where $\dot{\mathbf{X}} \in \mathbb{R}^{N \times J}$ is the matrix of derivatives that can be either measured or numerically obtained, $\Theta(\mathbf{X}, \mathbf{U}) \in \mathbb{R}^{N \times P}$ is the augmented matrix obtained by evaluating \mathbf{X} and \mathbf{U} using $\theta(\mathbf{x}, \mathbf{u})$, and $\mathbf{E} = [\boldsymbol{\varepsilon}_1 \ \boldsymbol{\varepsilon}_2 \ \dots \ \boldsymbol{\varepsilon}_J] \in \mathbb{R}^{N \times J}$ is the error matrix. Thus, for $j \in \mathcal{J}$, we formulate the problem as:

$$\min_{\langle \boldsymbol{\xi}_j, \boldsymbol{\gamma}_j \rangle} \|\dot{\mathbf{x}}_j - \Theta(\mathbf{X}, \mathbf{U})(\boldsymbol{\gamma}_j \circ \boldsymbol{\xi}_j)\|_2^2 + \lambda_2 \|\boldsymbol{\xi}_j\|_2^2 + \lambda_0 \|\boldsymbol{\xi}_j\|_0, \quad (13)$$

where $\boldsymbol{\gamma}_j \circ \boldsymbol{\xi}_j$ is the element-wise product (Hadamard product) of $\boldsymbol{\gamma}_j$ and $\boldsymbol{\xi}_j$, $\|\boldsymbol{\xi}_j\|_0$ is the ℓ_0 -norm (pseudo norm) that counts the number of nonzero entries of $\boldsymbol{\xi}_j$, $\|\boldsymbol{\xi}_j\|_2^2$ is the ℓ_2 -norm for reducing the effects from noisy data, and λ_0 and λ_2 are the associated regularization strengths.

The goal of system identification for the dynamic system in Eq. (13) is to correctly identify $\boldsymbol{\gamma}_j$ and calculate the coefficients $\boldsymbol{\xi}_j$ from measurement data \mathbf{X} and/or $\dot{\mathbf{X}}$. Existing works on sparse identification of dynamic systems, e.g., [20, 23-25], perform term selection and promote sparsity by imposing penalties on the coefficients. Stated differently, these methods try to identify the product $\boldsymbol{\gamma}_j \circ \boldsymbol{\xi}_j$ as a whole. Notwithstanding the success of these methods, they are usually very sensitive to noisy measurements [21]. The failure of previous methods to handle highly noisy measurement provided the motivation of the proposed physics-informed machine learning algorithm so to identify $\boldsymbol{\gamma}_j$ and $\boldsymbol{\xi}_j$ separately, where $\boldsymbol{\gamma}_j$ is identified by solving a discrete optimization problem. Equivalently, Eq. (13) is reformulated as the following discrete optimization problem to obtain $\boldsymbol{\gamma}_j$ and $\boldsymbol{\xi}_j$ for $f_j(\mathbf{x}, \mathbf{u})$:

$$\langle \boldsymbol{\xi}_j^*, \boldsymbol{\gamma}_j^* \rangle = \operatorname{argmin}_{\langle \boldsymbol{\xi}_j, \boldsymbol{\gamma}_j \rangle \in \Delta} \|\dot{\mathbf{x}}_j - \Theta(\mathbf{X}, \mathbf{U})(\boldsymbol{\gamma}_j \circ \boldsymbol{\xi}_j)\|_2^2 + \lambda_2 \|\boldsymbol{\xi}_j\|_2^2 \quad (14a)$$

and the solution space Δ is defined as

$$\Delta := \{ \langle \boldsymbol{\xi}_j, \boldsymbol{\gamma}_j \rangle \mid -M\boldsymbol{\gamma}_j \leq \boldsymbol{\xi}_j \leq M\boldsymbol{\gamma}_j, \boldsymbol{\gamma}_j^T \mathbf{e} = \kappa_j, \boldsymbol{\xi}_j \in \mathbb{R}^{P \times 1}, \boldsymbol{\gamma}_j \in \mathbb{B}^{1 \times P} \}, \quad (14b)$$

where M is the upper bound of $\boldsymbol{\xi}_j$ and can be initially set as $M = \|\boldsymbol{\xi}_j\|_\infty$. Constraints $-M\boldsymbol{\gamma}_j \leq \boldsymbol{\xi}_j \leq M\boldsymbol{\gamma}_j$ indicate the element-wise relationship between $\boldsymbol{\xi}_j$ and $\boldsymbol{\gamma}_j$. That is, if $\gamma_{pj} = 0$, then $\xi_{pj} = 0$; otherwise ξ_{pj}

is optimized within the interval $[-M, M]$. In constraint $\boldsymbol{\gamma}_j^T \mathbf{e} = \kappa_j$, $\mathbf{e} \in \mathbb{R}^{P \times 1}$ is a vector with all entries set to 1, and κ_j now refers to the number of non-zero terms in $f_j(\mathbf{x}, \mathbf{u})$. As such, through the determination of the value of κ_j , one can explicitly control the sparsity of the governing equations for a given dynamic system.

We propose a two-stage optimization algorithm to solve the problem (14). This method separates term identification for $\boldsymbol{\gamma}_j$ from coefficient estimation for $\boldsymbol{\xi}_j$ as outlined below.

Stage I: Term identification. This stage only determines the estimate of the optimal term combination, $\hat{\boldsymbol{\gamma}}_j^*$, by solving problem (14) using column-wise normalized data $\tilde{\boldsymbol{\Theta}}(\mathbf{X}, \mathbf{U})$ and $\tilde{\mathbf{x}}$. Normalization removes the effects of different scales on the determination of $\hat{\boldsymbol{\gamma}}_j^*$. The corresponding coefficient estimates $\hat{\boldsymbol{\xi}}_j$ are not used as the final solution.

Stage II: Coefficient estimation. Once $\hat{\boldsymbol{\gamma}}_j^*$ is identified, the optimal coefficients estimation $\hat{\boldsymbol{\xi}}_j^*$, is obtained with a least squares algorithm using the original data $\boldsymbol{\Theta}(\mathbf{X}, \mathbf{U})$ and $\dot{\mathbf{x}}_j$. Only columns in $\boldsymbol{\Theta}(\mathbf{X}, \mathbf{U})$ corresponding to nonzero values in $\hat{\boldsymbol{\gamma}}_j^*$ are used for regression. The use of the original data allows the acquired model $\hat{f}_j(\mathbf{x}, \mathbf{u})$ to consider the original scales of the data from the practical dynamic system before normalization.

Once $\hat{\boldsymbol{\gamma}}_j^*$ and $\hat{\boldsymbol{\xi}}_j^*$ are determined for $j \in \mathcal{J}$, the acquired model of the studied dynamic system is written as

$$\dot{\mathbf{x}} = \hat{\mathbf{f}}^*(\mathbf{x}, \mathbf{u}) = \boldsymbol{\theta}(\mathbf{x}, \mathbf{u})(\hat{\boldsymbol{\Gamma}}^* \circ \hat{\boldsymbol{\Xi}}^*), \quad (15)$$

where $\hat{\boldsymbol{\Gamma}}^*$ and $\hat{\boldsymbol{\Xi}}^*$ are constructed by stacking $\hat{\boldsymbol{\gamma}}_j^*$ and $\hat{\boldsymbol{\xi}}_j^*$, respectively. Advanced parameter-tuning techniques for determining κ_j and λ_2 can also be integrated accordingly [21].

3.2 Learning-based model predictive control

Once the model of the dynamic system is acquired, it can be used for system control by MPC. We

outline the MPC procedure based on the acquired model in this section. In the following steps, the discrete-time dynamic system form $\mathbf{x}_{k+1} = \hat{\mathbf{F}}^*(\mathbf{x}_k, \mathbf{u}_k)$ is used. MPC employs a basic concept of iteratively updating model states with instantly measured system responses then solving the resulting optimal control problem over a receding horizon. At time step k , current measurement \mathbf{x}_k is obtained. Then, a control sequence for the prediction horizon of H time steps, $\mathbf{u}(\cdot | \mathbf{x}_k) = \{\mathbf{u}_{k+1}, \mathbf{u}_{k+2}, \dots, \mathbf{u}_{k+H}\}$, is calculated by solving an open-loop optimal control problem considering future H steps using the acquired model. Next, the first value \mathbf{u}_{k+1} of the computed control sequence is applied to the system as the system advances one step. An updated system state measurement \mathbf{x}_{k+1} is then collected and used to reinitiate the model state.

Mathematically, at time step k where $k \in \mathcal{K} := \{1, \dots, K\}$ and K is the maximum number of steps during MPC, we solve the below optimal control problem using a discrete-time dynamic system form to determine \mathbf{u}_{k+1} :

$$\begin{aligned} \min_{\mathbf{u}} L &:= \sum_{i=1}^H \ell(\hat{\mathbf{x}}_{k+i}, \mathbf{u}_{k+i}, \mathbf{r}_{k+i}) & (16a) \\ s. t. \quad \hat{\mathbf{x}}_{k+i+1} &= \hat{\mathbf{F}}^*(\hat{\mathbf{x}}_{k+i}, \mathbf{u}_{k+i}), & \forall i = 0, \dots, H-1, & (16b) \\ \mathbf{h}_{\mathbf{x}}(\hat{\mathbf{x}}_{k+i}) &\leq \mathbf{0}, & \forall i = 0, \dots, H-1, & (16c) \\ \mathbf{h}_{\mathbf{u}}(\mathbf{u}_{k+i}) &\leq \mathbf{0}, & \forall i = 0, \dots, H-1, & (16d) \\ \mathbf{x}_k &\in \mathcal{X}_{init}, & & (16e) \end{aligned}$$

where $\hat{\mathbf{x}}_{k+i}$ is the model prediction of the state, \mathbf{x}_k is the given initial value for step k and $\hat{\mathbf{x}}_k = \mathbf{x}_k$. The objective of this formulation is to minimize the summation of cost $\ell(\hat{\mathbf{x}}_{k+i}, \mathbf{u}_{k+i}, \mathbf{r}_{k+i})$, at specific time epoch i over $i = 1, \dots, H$. The dynamic system model in constraints Eq. (16b) represents the discrete-time or discretized version of the acquired model in Eq. (15). Inequalities (16c) and (16d) represent the constraints for the system variables and control variables, respectively. These constraints are particularly important for practical engineering systems where the expensive control expenditure is usually avoided. Specific system requirements, such as stability, accuracy, and robustness can also be integrated into these hard constraints. Constraints (16e) denote the initial conditions at step k for \mathbf{x}_k belong to the feasible initial states \mathcal{X}_{init} .

Formulation (16) provides a general structure for model predictive control. The many possible designs of the objectives, controllers, and optimizers mean a broad spectrum of solution routines exist for solving problem (16). For example, one commonly used objective is of the form

$$L := \sum_{i=1}^H \|\hat{\mathbf{x}}_{k+i} - \mathbf{r}_{k+i}\|_{\mathbf{Q}}^2 + \|\mathbf{u}_{k+i}\|_{\mathbf{R}}^2, \quad (17)$$

where $\hat{\mathbf{x}}_{k+i} - \mathbf{r}_{k+i}$ relates to the deviation of the state \mathbf{x}_{k+i} to the commanded reference \mathbf{r}_{k+i} . Here we define $\|\mathbf{a}\|_{\mathbf{Q}}^2 = \mathbf{a}^T \mathbf{Q} \mathbf{a}$ as the weighted norm of vector $\mathbf{a} \in \mathbb{R}^{J \times 1}$, where $\mathbf{Q} \in \mathbb{R}^{J \times J}$ is a positive semi-definite weighting matrix for the state variables. In addition, the practical constraints of \mathbf{u}_{k+i} may lead to the expenditure of expensive control inputs. Thus, to manage expenditure it is common practice to include a regularization term for the control inputs \mathbf{u}_{k+i} in the second term, where $\mathbf{R} \in \mathbb{R}^{S \times S}$ is a positive semi-definite weighting matrix for the control inputs. Moreover, the inclusion of the regularization term may also be motivated by smoothness requirements for the control inputs. Consequently, the controller design relies heavily on the specific nonlinear dynamics and defined objective of the system. The control actions can be generally obtained in one of two ways: 1) direct computation of the sequence for optimal control inputs $\{\mathbf{u}_{k+1}, \mathbf{u}_{k+2}, \dots, \mathbf{u}_{k+H}\}$ by solving formulation (16), or 2) construction of an explicit parameterized control policy function $\pi_{\zeta}(\cdot)$ to thereby optimize its parameters to produce the control sequence, that is

$$\{\mathbf{u}_{k+1}, \mathbf{u}_{k+2}, \dots, \mathbf{u}_{k+H}\} = \pi_{\zeta}(\mathbf{x}_k, \mathbf{u}_k). \quad (18)$$

Representatives of the previously mentioned categories are MPC [20] and differentiable predictive control (DPC) [26]. For the studied dynamic systems in this paper, variants of MPC are implemented. For example, classical MPC is employed for the nonlinear chaotic Lorenz 3 system in Section 4.2. In Section 4.3, the specialty of turning dynamics stability requires that the system time step and control time step be different. Hence, a new adaptation of MPC formulation is adopted for stability-based control process parameters identification.

In closing, we summarize the algorithm procedure of PIMLC in Algorithm 1. The dynamic system

model $\dot{\mathbf{x}} = \hat{\mathbf{f}}^*(\mathbf{x}, \mathbf{u})$ is first acquired via the discrete optimization-based physics-informed machine learning algorithm, and model predictive control is applied to obtain the control sequence $\{\mathbf{u}_1, \mathbf{u}_2, \dots, \mathbf{u}_K\}$.

Algorithm 1. Physics-informed machine learning-based control (PIMLC) method.

Input: Time series measurements \mathbf{X}, \mathbf{U} and the computed or measured $\dot{\mathbf{X}}$;

Output: Set of equations $\dot{\mathbf{x}} = \hat{\mathbf{f}}^*(\mathbf{x}, \mathbf{u})$ and control sequence $[\mathbf{u}_1, \mathbf{u}_2, \dots, \mathbf{u}_K]$;

Function PIMLC($\mathbf{X}, \mathbf{U}, \dot{\mathbf{X}}$)

1. $\dot{\mathbf{x}} = \hat{\mathbf{f}}^*(\mathbf{x}, \mathbf{u}) \leftarrow$ **Physics-informed machine learning-based system identification**;
2. $[\mathbf{u}_1, \mathbf{u}_2, \dots, \mathbf{u}_K] \leftarrow$ **Learning-based model predictive control**;
3. **Return:** Set of equations $\dot{\mathbf{x}} = \hat{\mathbf{f}}^*(\mathbf{x}, \mathbf{u})$ and control sequence $[\mathbf{u}_1, \mathbf{u}_2, \dots, \mathbf{u}_K]$;

Function Physics-informed machine learning-based system identification($\mathbf{X}, \mathbf{U}, \dot{\mathbf{X}}$)

Initialize: Construct $\theta(\mathbf{x}, \mathbf{u})$ and $\Theta(\mathbf{X}, \mathbf{U})$; $\hat{\mathbf{F}}^* \leftarrow \mathbf{0}, \hat{\mathbf{E}}^* \leftarrow \mathbf{0}$;

Compute $\tilde{\Theta}(\mathbf{X}, \mathbf{U}), \tilde{\dot{\mathbf{X}}} \leftarrow$ Normalize $\Theta(\mathbf{X}, \mathbf{U})$ and $\dot{\mathbf{X}}$;

for $j \in \mathcal{J}$ **do**

$\hat{\mathcal{Y}}_j^* \leftarrow$ Stage I: solve problem (14) with $\tilde{\Theta}(\mathbf{X}, \mathbf{U})$ and $\tilde{\mathbf{x}}_j$;

$\hat{\xi}_j^* \leftarrow$ Stage II: estimate coefficients with $\Theta(\mathbf{X}, \mathbf{U})$ and $\hat{\mathcal{Y}}_j^*$;

Return: set of acquired models $\dot{\mathbf{x}} = \hat{\mathbf{f}}^*(\mathbf{x}, \mathbf{u}) = \theta(\mathbf{x}, \mathbf{u})(\hat{\mathbf{F}}^* \circ \hat{\mathbf{E}}^*)$.

Function Learning-based model predictive control ($\dot{\mathbf{x}} = \hat{\mathbf{f}}^*(\mathbf{x}, \mathbf{u})$)

Initialize: Construct the optimal control problem (16) using $\dot{\mathbf{x}} = \hat{\mathbf{f}}^*(\mathbf{x}, \mathbf{u})$.

For $k \in \mathcal{K}$ **do**

$\{\mathbf{u}_{k+1}, \mathbf{u}_{k+2}, \dots, \mathbf{u}_{k+H}\} \leftarrow$ Solve problem (16);

Select \mathbf{u}_{k+1} to apply and obtain new measurement \mathbf{x}_{k+1} ;

Return: control sequence $\{\mathbf{u}_1, \mathbf{u}_2, \dots, \mathbf{u}_K\}$.

4. Simulation Results

This section presents the simulation results of the proposed PIMLC method from two perspectives: the accuracy of the system identification, and the effectiveness of the model predictive control. The testbeds include the classical chaotic Lorenz 3 system and the sim-to-real simulator of a practical dynamic system, the turning machine tool. For all the example systems, the experiments are deployed on a mobile workstation with Intel XI(R) W-10885M CPU @ 2.40GHz, 128 GB memory, and the 64-bit Windows 10 Pro operating system for workstations.

4.1 Numerical experiment settings

Noisy data. We generate data with noise to validate the robustness of system identification for the proposed PIMLC method. For all simulations, the time series data matrices \mathbf{X} , \mathbf{U} and/or $\dot{\mathbf{X}}$ are generated from the numerical solutions of the governing equations. For the scenario where both the state variables \mathbf{x} and their derivatives $\dot{\mathbf{x}}$ can be measured, the Gaussian noise is added to $\dot{\mathbf{x}}$, that is,

$$\dot{\mathbf{x}}_j^{\text{Noise}} = \dot{\mathbf{x}}_j + r\sigma_{\dot{\mathbf{x}}_j}\boldsymbol{\epsilon}, \quad \forall j \in \mathcal{J}, \quad (19)$$

where $\dot{\mathbf{x}}_j \in \mathbb{R}^{N \times 1}$ is the j -th column of measured derivative matrix $\dot{\mathbf{X}}$, $\sigma_{\dot{\mathbf{x}}_j}$ is the standard deviation of column $\dot{\mathbf{x}}_j$, r is the ratio of noise level with respect to $\sigma_{\dot{\mathbf{x}}_j}$, and $\boldsymbol{\epsilon} \in \mathbb{R}^{N \times 1}$ is a vector with each entry following the standard normal distribution $\mathcal{N}(0,1)$. With such noise settings, a larger r indicates larger noise in the data.

Performance metrics. We evaluate the performance of the proposed PIMLC from both the system identification and model predictive control aspects. The comparison methods include those previously studied [20], including SINDY-MPC and a nonlinear autoregressive network with exogenous inputs (NARX) integrated with MPC (NARX-MPC).

For system identification, we examine the capability of the methods under comparison for exact identification of the target dynamic system from noisy data. This is defined by the number of exactly acquired equations as below:

$$A(\boldsymbol{\Gamma}) := \sum_{j=1}^J \mathbf{1}_{\hat{\boldsymbol{\gamma}}_j^* = \boldsymbol{\gamma}_j^\dagger} = \begin{cases} 1, & \text{if } \hat{\boldsymbol{\gamma}}_j^* = \boldsymbol{\gamma}_j^\dagger, \\ 0, & \text{if } \hat{\boldsymbol{\gamma}}_j^* \neq \boldsymbol{\gamma}_j^\dagger, \end{cases} \quad (20)$$

where $\hat{\boldsymbol{\gamma}}_j^*$ is identified by the tested method and $\boldsymbol{\gamma}_j^\dagger$ is the ground truth of the target dynamic system. The exact identification of the dynamic system occurs when $A(\boldsymbol{\Gamma}) = J$. Upon exact identification, we further evaluate the accuracy of the estimated coefficients. Note the above $A(\boldsymbol{\Gamma})$ can only be used for comparison between PIMLC and SINDY-MPC as both can identify the analytical form of the governing equation.

Whereas the resultant trajectories are used to evaluate the comparison between PIMLC and NARX-MPC.

For model predictive control, the primary performance metric is the steady state error. This error measures the difference between the steady state response and the desired control reference. Numerically, we define the e_{ss} as the sum of squared errors at the steady state:

$$e_{ss} := \frac{1}{N_f J} \sum_{k=N_0+1}^{N_0+N_f} \| \mathbf{x}_k - \mathbf{r}_k \|_2^2, \quad (21)$$

Where N_0 is a positive time point after which the dynamic system model is at its steady state, and N_f is the number of measurements used for calculation. A smaller e_{ss} indicates a smaller average distance of the steady state output from the desired value. Thus, the smaller the steady state error the better control performance of the method.

Algorithm implementation. In Algorithm 1, the mixed integer linear programming (MILP) solver with branch and cut algorithm in CPLEX 20.1, is used to solve the problem in Eqs. (14) with the Python interface *docplex*. Unless otherwise noted, the parameters for PIMLC in the system identification procedure are as follows: $M = 1000$, $\lambda_2 = \sigma_{\dot{x}_j} / \sqrt{N}$, and κ_j is set as the number of terms of the ground truth. After the model is acquired, it is implemented in MATLAB for MPC to harness the strength of the MATLAB embedded nonlinear optimization solver *fmincon*. Sequential quadratic programming (SQP) is chosen as the optimizer for solving problem (16). For SQP, we construct the objective of problem (16) to be twice continuously differentiable. For the benchmarks, we adopt PySINDy from Python and the MATLAB function *narxnet* for SINDY-MPC and NARX-MPC, respectively.

4.2 The Lorenz 3 system

The chaotic Lorenz 3 system with control is described by the below state space model with three state variables:

$$\dot{x}_1 = \alpha(x_2 - x_1) + u, \quad (22a)$$

$$\dot{x}_2 = x_1(\rho - x_3) - x_2, \quad (22b)$$

$$\dot{x}_3 = x_1x_2 - \beta x_3. \quad (22c)$$

The following system parameter settings are selected to ensure chaotic behavior: $\alpha = 10, \beta = 8/3$, and $\rho = 28$. The Schroeder Phased Harmonic Signal (sphs) control signal is used for training data generation, where actuation is only added to x_1 . The dataset is generated using the initial condition $\mathbf{x}_0 = (-8, 8, 27)^T$ and the time step $\Delta t = 0.001$ in $t \in [0, 10]$ time units. As for the candidate terms construction, we set the maximum polynomial order to two and get a dictionary of 15 candidate terms in total. The hard threshold of coefficients in SINDY-MPC is set to 0.1. The model structure of NARX is set as [4, 10, 3] (four input nodes, one hidden layer with ten nodes, and three output nodes).

For MPC, both constant set point and trajectory control are conducted. For the constant set point regulation, the control goal is to stabilize the trajectory to one of the two fixed points, $(-\sqrt{72}, -\sqrt{72}, 27)^T$. The parameter settings are as follows: $H = 10$, $\mathbf{Q} = \mathbf{I}_{3 \times 3}$, $\mathbf{R} = 0.001$, and $[L_{\mathbf{u}}, U_{\mathbf{u}}] = [-50, 50]$. For the trajectory tracking control, the planned trajectory for x_1 is set as $\mathbf{r}(t) = 2 \sin(7t)$, $H = 10$, $\mathbf{Q} = \text{diag}(500, 0, 0)$, $\mathbf{R} = 0.001$, and $[L_{\mathbf{u}}, U_{\mathbf{u}}] = [-200, 200]$. It is noted here that different time steps are utilized for the control optimizer and the system evolution. In particular, the time step for the system evolution is $\Delta t_{\text{sys}} = 0.001$, and that for the MPC optimizer is $\Delta t_{\text{MPC}} = 0.01$. That is, at each control time step, the optimized control input will be applied as a constant control signal over a system evolution of 10 steps, with each system time step equal to 0.001. The purpose of these settings is to balance the length of the prediction horizon with system evolution accuracy, as Lorenz 3 is a chaotic system and a larger time step for the numerical solution will lead to long-term prediction error.

Table 1 shows the system identification results with metric $A(\Gamma)$ for the Lorenz system by comparing PIMLC with SINDY-MPC. The PIMLC method significantly outperforms the SINDY-MPC method as evidenced by the largest noise ratio for accurate identification of PIMLC is 10 times larger than that of SINDY-MPC. For MPC analysis we choose the acquired models by SINDY-MPC and PIMLC at

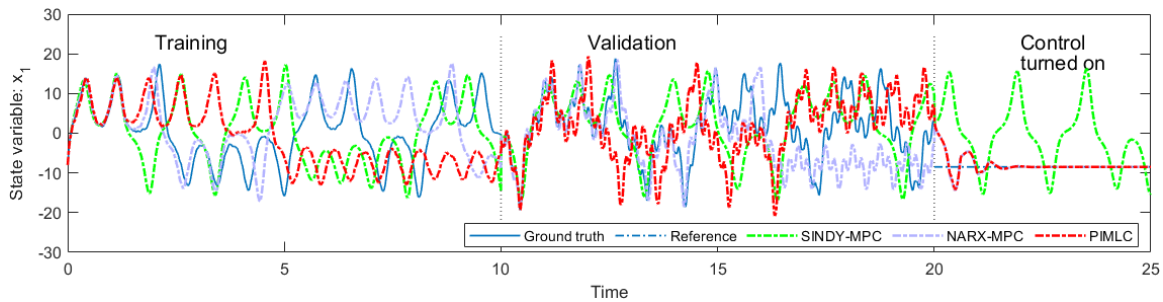
noise ratio $r = 100\%$. The results from MPC analysis for the models are presented in Table 2. It is observed that the identified coefficients of PIMLC deviate slightly from the ground truth, whereas the results from SINDY-MPC include many redundant terms.

Table 1. System identification performance by the number of exactly acquired equations $A(\Gamma)$ for Lorenz 3 system. The equations in the grey cells are used for control, see Table 2.

Noise ratio: r	SINDY-MPC	PIMLC
0%	3	3
10%	3	3
30%	2	3
50%	1	3
70%	1	3
100%	1	3
1000%	0	1
5000%	0	0

Table 2. Acquired equations under noise ratio $r = 100\%$ for the chaotic Lorenz 3 system

Ground truth	$\dot{x}_1 = 10x_2 - 10x_1 + u$ $\dot{x}_2 = 28x_1 - x_1x_3 - x_2$ $\dot{x}_3 = x_1x_2 - 8/3x_3$
SINDY-MPC	$\dot{x}_1 = 10.2052x_2 - 10.2517x_1 + 1.1976u$ $\dot{x}_2 = 28.3417x_1 - 1.6062x_2 + 0.5-59u - 0.9934x_1x_3$ $\dot{x}_3 = 1.2545x_1 - 0.8872x_2 - 2.8931x_3 + 0.5186u + 1.0532x_1x_2 - 0.2276x_1u + 0.1173x_2u$
PIMLC	$\dot{x}_1 = 10.2052x_2 - 10.2517x_1 + 1.1976u$ $\dot{x}_2 = 28.8872x_1 - 1.8023x_2 - 1.0040x_1x_3$ $\dot{x}_3 = 1.0528x_1x_2 - 2.7880x_3$



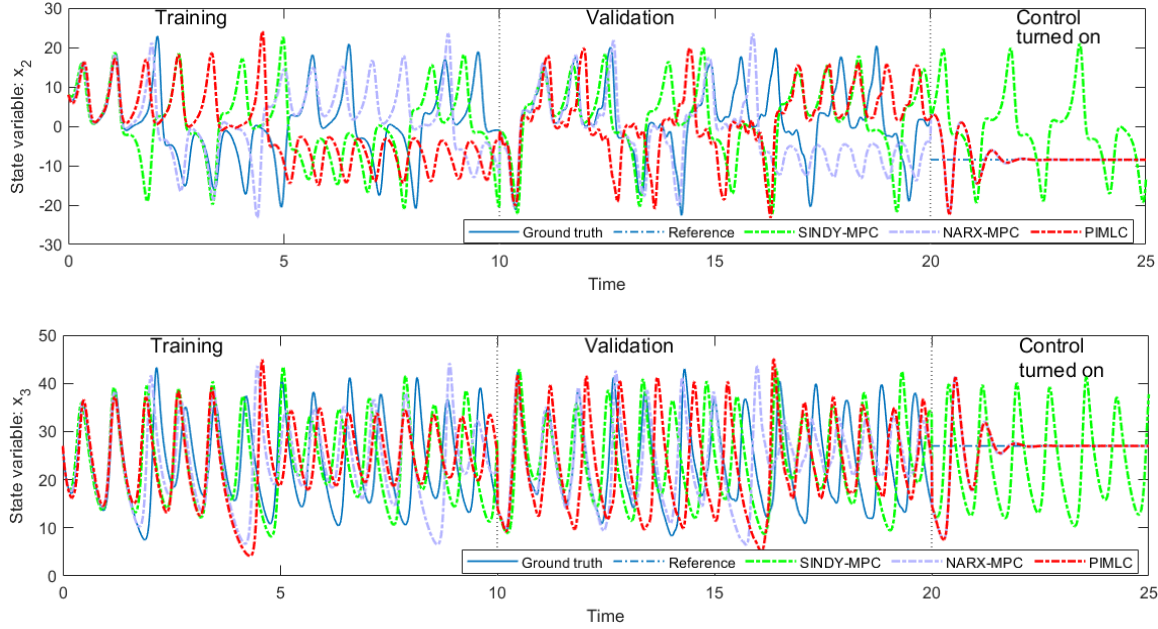


Fig. 2. Simulation results comparison of constant set point control for Lorenz 3 system using the model acquired at noise ratio $r = 100\%$.

Fig. 2 depicts the simulation results for constant set point control. For the training stage, we evolve the acquired models for 10 time units using the same controller as training data. A separate, new controller $u(t) = (5 \sin^3(30t))$ is used to evolve another 10 time units for the model validation stage. Last, MPC is used to drive system evolution for another 5 time units. Results from all three methods fail to align closely with the ground truth trajectories for both training and validation stages, with an exception to the beginning of each simulation. With increases in time, it seems that the chaotic behavior of the Lorenz 3 system leads to significant deviations for all three trajectories. That said, the MPC stage demonstrates the strong performance of PIMLC for data-driven control. SINDY-MPC exhibits poor performance, as observed by nonconvergence of state variables to the desired reference values. Of particular interest, NARX-MPC exhibits MPC performance similar to that of PIMLC. This is evidenced by near overlapping trajectories for x_1, x_2 and x_3 across NARX-MPC and PIMLC. This result indicates that the NARX model indeed captures the dynamics of Lorenz 3, although as a black-box model. Results as measured by steady state error e_{SS} are shown in Table 3. SINDY-MPC has the largest steady state error followed by NARX-MPC and the smallest

error observed from PIMLC. Worthy of note, the steady state error of PIMLC is roughly 69% of error recorded from NARX-MPC. In brief, PIMLC yields the best performance for MPC, followed by NARX-MPC and then SINDY-MPC.

Table 3. MPC performance comparison of constant set point control by steady state error e_{ss} for chaotic Lorenz 3 system.

Method	SINDY-MPC	NARX-MPC	PIMLC
e_{ss}	99.1787	2.0508E-04	1.4028E-04

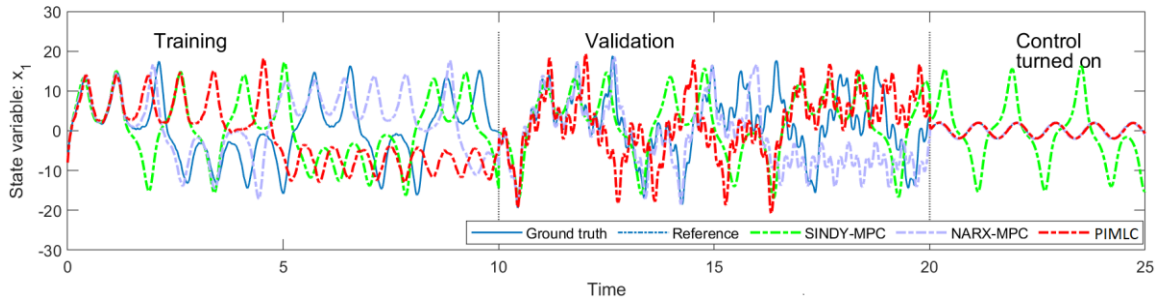


Fig. 3. Simulation results comparison of trajectory tracking control for Lorenz 3 system using acquired model at noise ratio $r = 100\%$

Table 4. MPC performance comparison of trajectory tracking control by steady state error e_{ss} for chaotic Lorenz 3 system.

Method	SINDY-MPC	NARX-MPC	PIMLC
e_{ss}	70.1927	0.0134	0.0085

Fig. 3 displays the trajectory tracking control results for Lorenz 3 system and Table 4 shows the corresponding results for e_{ss} . Note here e_{ss} is calculated by only considering x_1 since x_1 is the only variable to be tracked in the objective. Best control performance is obtained by PIMLC as observed by the model completely overlapping with the demanded trajectory (Reference is the blue dashed line in the figure). This is followed by NARX-MPC and then SINDY-MPC. The steady state error of PIMLC is recorded to be roughly 63% of error for NARX-MPC. In stark contrast, SINDY-MPC completely fails to track the planned trajectory.

To summarize, the proposed PIMLC exhibits 10 times better anti-noise capability than SINDY-MPC for accurate modeling. For control, PIMLC performs seven and four orders of magnitude better than

SINDY-MPC for constant set point and trajectory tracking control, respectively. Altogether, PIMLC demonstrates greater performance for both data-driven modeling and control under high-noise conditions.

4.3 Turning machine tool

In machine tool research, the equation of motion for the dynamics of a turning machine tool [27-29] can be modeled as

$$m\ddot{y} + c\dot{y} + ky = F_n = K_s b (h_m + y(t - \tau) - y(t)) \cos \beta, \quad (23)$$

where y , \dot{y} , and \ddot{y} are the displacement, velocity and acceleration, of the vibration caused by cutting force F_n (N). The mass, linear spring constant and viscous damping coefficient are denoted as m (kg), k (N/m) and c (N s/m). The left-hand-side of Eq. (23) describes the system dynamics while the right-hand-side shows a force model. The mean chip thickness h_m and time delay term $y(t - \tau) - y(t)$ indicate the varying instantaneous chip thickness and determine the instantaneous normal cutting force F_n with angle β (degree). $\tau = 1/\Omega$ is the time per rotation, $t - \tau$ indicates the time delay term, and K_s is a process dependent coefficient (N/mm²) depending on the workpiece materials and tool geometry. The two cutting parameters considered in this paper are chip width b (mm) and spindle rate Ω (rps).

The training data is generated using time domain simulation, which solves equation (24) based on Euler integration [27]. This time domain simulation has been well validated for high accuracy and good agreement with the physical turning machine tool [28]. Under high-speed settings, process damping is insignificant. Thus, the time domain simulation of Eq. (23) is a high-fidelity sim-to-real simulator which can be regarded as a surrogate for experiments. Accordingly, a set of $\langle \Omega, b \rangle$ combinations are sampled for both stable and unstable high-speed cutting operations, where $\Omega \in \{400, 600, 800\}$ rps and $b \in \{2, 8\}$ mm. The measurements include y , \dot{y} , \ddot{y} and F_n , and all are contaminated with Gaussian noise. In practice, y , \dot{y} , \ddot{y} and F_n can be measured using advanced metrology. For example, a capacitance probe, a laser vibrometer, a low mass accelerometer and a dynamometer can be used to measure y , \dot{y} , \ddot{y} and F_n , respectively. For each combination of $\langle \Omega, b \rangle$, the first 2000 data points, which contain rich transient nonlinear dynamics, are used

for training. The parameters used for simulation are as follows: $m = 3.17$ kg, $k = 2 \times 10^7$ N/m, $c = 795.77$ N/m², $K_s = 1500$ N/mm², $h_m = 0.1$ mm, $\beta = 68$ deg and $n_{rev} = 100$ for number of revolutions. Accordingly, the natural frequency $f_n = 400$ Hz, the damping ratio $\zeta = 0.05$ and the time step $\Delta t = 1.25 \times 10^{-5}$ s.

For system identification, the system dynamics and force models are acquired separately. For the system dynamics, the second order polynomial of $[y \dot{y} \ddot{y}]$ is constructed to include 10 candidate terms (including constant). For the force model, we include an additional time delay term $y(t) - y(t - \tau)$. The threshold of SINDY-MPC is tuned to 0.01 and 0.005 for the system dynamics and the force model, respectively. We do not report the results for NARX since the acquired model is a black-box model and cannot be used for subsequent stability analysis.

For MPC, we treat the cutting parameters $\langle \Omega, b \rangle$ as control parameters \mathbf{u} . The objective of model-based control is to select the cutting parameters $\langle \Omega^*, b^* \rangle$ that are stable while maximizing the material removal rate (MRR), subject to the acquired governing equations in the forms of Eq. (23). During the sequential optimization of MPC, for arbitrary $\langle \Omega_l, b_l \rangle$ where $l = k + 1, \dots, k + H$, the dynamic system model must be evolved until the stability of $\langle \Omega_l, b_l \rangle$ can be identified. Mathematically, the optimal control problem can be formulated as

$$\max_{\langle \Omega, b \rangle} L := \sum_{l=k+1}^{k+H} MRR_l^2 = \sum_{l=k+1}^{k+H} h_m^2 \Omega_l^2 b_l^2 \quad (24a)$$

$$s. t. \hat{y}_{j+1}^l = \hat{y}_j^l + \frac{1}{\Omega_l N_\tau} \hat{z}_j^l, \quad \forall l = k + 1, \dots, k + H, \quad (24b)$$

$$\hat{z}_{j+1}^l = \hat{z}_j^l + \frac{1}{\Omega_l N_\tau} \left(-\frac{c}{m} \hat{z}_j^l - \frac{k}{m} \hat{y}_j^l + \frac{K_s b_l}{m} (h_m + \hat{y}_{j-N_\tau}^l - \hat{y}_j^l) \right), \quad \forall l = k + 1, \dots, k + H, \quad (24c)$$

$$\frac{1}{N} \sum_{i=N_0+1}^{N_0+N_f} (\hat{y}_{iN_\tau}^l - \hat{y}_{(i-1)N_\tau}^l)^2 \leq M_0, \quad \forall l = k + 1, \dots, k + H, \quad (24d)$$

$$\Omega_l \in [L_\Omega, U_\Omega], \quad \forall l = k + 1, \dots, k + H, \quad (24e)$$

$$b_l \in [L_b, U_b], \quad \forall l = k + 1, \dots, k + H, \quad (24f)$$

$$\langle y_0^l, z_0^l \rangle \in \mathcal{Y}_{init}^l, \quad \forall l = k + 1, \dots, k + H, \quad (24g)$$

where \hat{y}_j^l, \hat{z}_j^l are the predictions for displacement and velocity, of the tool vibration at discretization step j

under parameters $\langle \Omega_l, b_l \rangle$. The objective (24a) is set as the sum of squares of the material removal rate (MRR), $MRR_l = h_m \Omega_l b_l$, with unit mm²-rps for parameters $\langle \Omega_l, b_l \rangle$. Constraints (24b) and (24c) form the discrete state-space model for the canonical form of the equation of motion in Eq. (23). Since the cycle time per revolution is $1/\Omega_l$ (s), the time step for the dynamic system model evolution can be calculated by $\Delta t = 1/(\Omega_l N_\tau)$, where N_τ is the number steps per revolution. Consequently, $\hat{y}_{j-N_\tau}^l$ is the displacement one revolution before step j and $\hat{y}_{j-N_\tau}^l - \hat{y}_j^l$ is the time delay term. Based on the time delay term, the stability metric in constraint (24d) is defined as

$$M := \frac{1}{N} \sum_{i=N_0+1}^{N_0+N_f} (\hat{y}_{iN_\tau}^l - \hat{y}_{(i-1)N_\tau}^l)^2, \quad (25)$$

where the displacement $\hat{y}_{iN_\tau}^l$ is obtained by once-per-revolution sampling. That is, starting from revolution $N_0 + 1$ where N_0 is large enough to reach the steady state of the system evolution, N displacements $\hat{y}_{iN_\tau}^l$ are periodically sampled. The sum of squared differences between successively sampled points is averaged and compared with a defined threshold, M_0 . For stable cuts, the sampled points are close to each other, so $M \leq M_0$ with M ideally equaling zero. For unstable cuts, however, $M > M_0$.

The parameter settings for formulation (24) are as follows: $K = 5$, $N_0 = 180$, $N_f = 20$, $N_\tau = 20$. The threshold for the stability metric is set as $M_0 = 2\text{E-}16$. To decrease the computational instability of numerical precision in MATLAB caused by small values of M and M_0 , the hard constraint (24d) is implemented by multiplying a large positive constant on both sides of the inequality. That is, $\lambda(M - M_0) \leq 0$, where $\lambda = 1\text{E}12$. The lower and upper bounds for the simulation are $[L_\Omega, U_\Omega] = [430, 800]$ rps, $[L_b, U_b] = [2, 8]$ mm. The initial condition $\langle y_0^l, z_0^l \rangle$ is set as the last values of displacement and velocity under $\langle \Omega_k^*, b_k^* \rangle$. The stopping criteria include both the maximum number of iterations $K = 30$ for MPC, and the change of the objective such that $\Delta L \leq 0.01$, whichever is satisfied at first.

We first present the results for system identification under different noises by the number of correctly acquired equations, $A(\Gamma)$, followed by the frequency domain analysis of the acquired model.

Then, we show the acquired model can be used for MPC to identify the best cutting parameters.

Table 5. Number of exactly acquired equations ($A(\Gamma)$) under different $\langle \Omega, b \rangle$ combinations.

Noise ratio: r	Cutting parameters combination $\langle \Omega, b \rangle$											
	400,2		400,8		600,2		600,8		800,2		800,8	
	SINDY-MPC	PIMLC	SINDY-MPC	PIMLC	SINDY-MPC	PIMLC	SINDY-MPC	PIMLC	SINDY-MPC	PIMLC	SINDY-MPC	PIMLC
0%	1	1	1	1	1	1	1	1	1	1	1	1
0.01%	1	1	1	1	1	1	0	1	1	1	1	1
0.1%	1	1	1	1	1	1	0	1	0	1	0	1
1%	0	1	1	1	0	1	0	1	0	1	0	1
10%	0	1	0	1	0	1	0	1	0	1	0	1
50%	0	1	0	1	0	1	0	0	0	1	0	0
100%	0	1	0	1	0	0	0	0	0	0	0	0
500%	0	0	0	0	0	0	0	0	0	0	0	0

Table 6. PIMLC acquired equation of motion under $\langle \Omega, b \rangle = \langle 400, 2 \rangle$. The equation in the grey cell is chosen for the subsequent MPC.

Noise ratio: r	Acquired equation of motion
0%	$3.17\ddot{y} + 795.77\dot{y} + 20000000.00y = 0.0562b + 561.9099b(y(t) - y(t - 1/\Omega))$
0.01%	$3.17\ddot{y} + 795.80\dot{y} + 19999995.98y = 0.0562b + 561.9013b(y(t) - y(t - 1/\Omega))$
0.1%	$3.17\ddot{y} + 795.99\dot{y} + 19999959.29y = 0.0562b + 561.8236b(y(t) - y(t - 1/\Omega))$
1%	$3.17\ddot{y} + 797.92\dot{y} + 19999545.78y = 0.0562b + 560.9935b(y(t) - y(t - 1/\Omega))$
10%	$3.16\ddot{y} + 816.41\dot{y} + 19990743.96y = 0.0562b + 547.5045b(y(t) - y(t - 1/\Omega))$
50%	$3.03\ddot{y} + 879.00\dot{y} + 19850816.84y = 0.0561b + 405.2419b(y(t) - y(t - 1/\Omega))$
100%	$2.74\ddot{y} + 911.24\dot{y} + 19464876.70y = 0.0561b + 201.0747b(y(t) - y(t - 1/\Omega))$

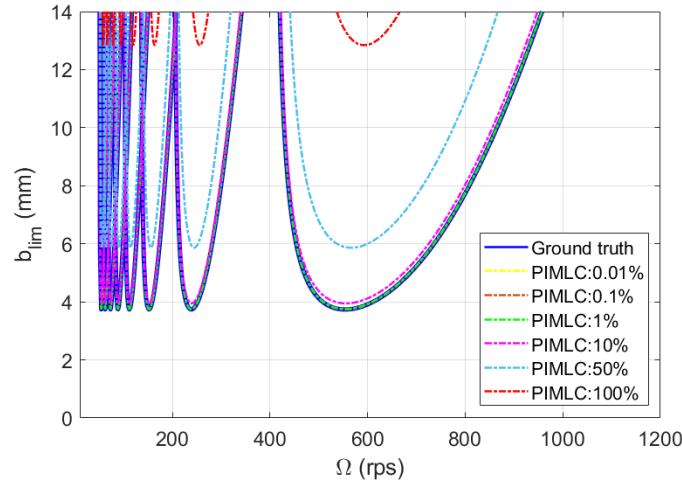


Fig. 4. The stability lobe diagrams for $\langle \Omega, b \rangle = \langle 400, 2 \rangle$ in Table 6. The stability lobes under noises 0.01%, 0.1% and 1% are almost perfectly overlapped with those of noise-free 0.00% (ground truth).

Table 5 shows the values of $A(\Gamma)$ for turning dynamics at 6 different combinations of $\langle \Omega, b \rangle$ under noise levels ranging from 0.01% to 500%. The bold **1** indicates that the equation of motion in the form of (23) is correctly acquired. PIMLC significantly outperforms SINDY-MPC, as evidenced by the failure of SINDY-MPC to identify the equations from data with any noise ratio greater than 1%, whereas, PIMLC can identify the equations from data generated using a noise ratio up to 100%. Within a specific Ω , lower values of b lead to better performance. That is, we can utilize lower values of Ω and b to collect highly effective in-process data. This can be used to guide experimental data collection for practical implementation of PIMLC.

Using the acquired equations of motion of parameters $\langle \Omega, b \rangle = \langle 400, 2 \rangle$ under different noises, see grey cells in Table 6, we perform frequency analysis to obtain the stability lobe diagrams, see Fig. 4. As the noise level increases the coefficients of the acquired equation of motion gradually deviate from the ground truth (0.00% noise). This deviation results in an increased damping estimate, and decreased mass and stiffness estimates. Accordingly, the resulting stability lobes in Fig. 4 shift upward and to the right.

Fig. 4 is an illustration of the good interpretability of the generated PIMLC models in two ways. First, the coefficients of the terms \ddot{y} , \dot{y} , and y represent specific physical meanings for mass, linear spring dynamics and damping, each of which inherently describes the mechanical properties of the turning machine. Second, based on the linear form of the discovered system dynamics and time-delayed force model, frequency analysis can be conducted for machining stability. In other words, white-box models with good interpretability allow for the potential for subsequence analysis; however, black-box models are unable to provide similar levels of interpretation, thereby limiting follow-up analyses. Due to the inferior performance of SINDY-MPC for identifying white-box models, we do not include those results in this paper.

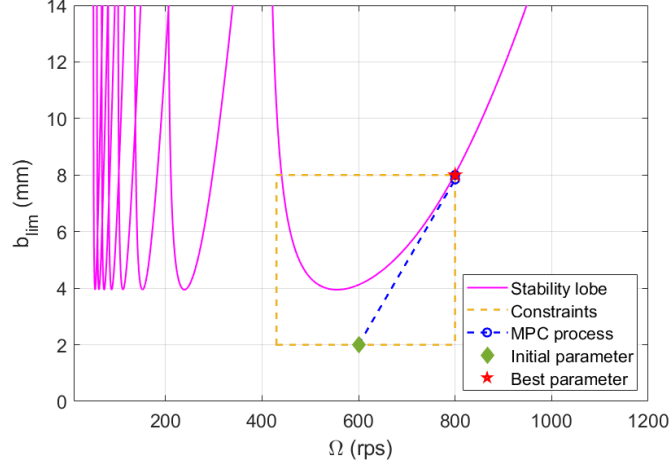


Fig. 5. The MPC result for turning dynamics using model acquired at noise ratio $r = 10\%$.

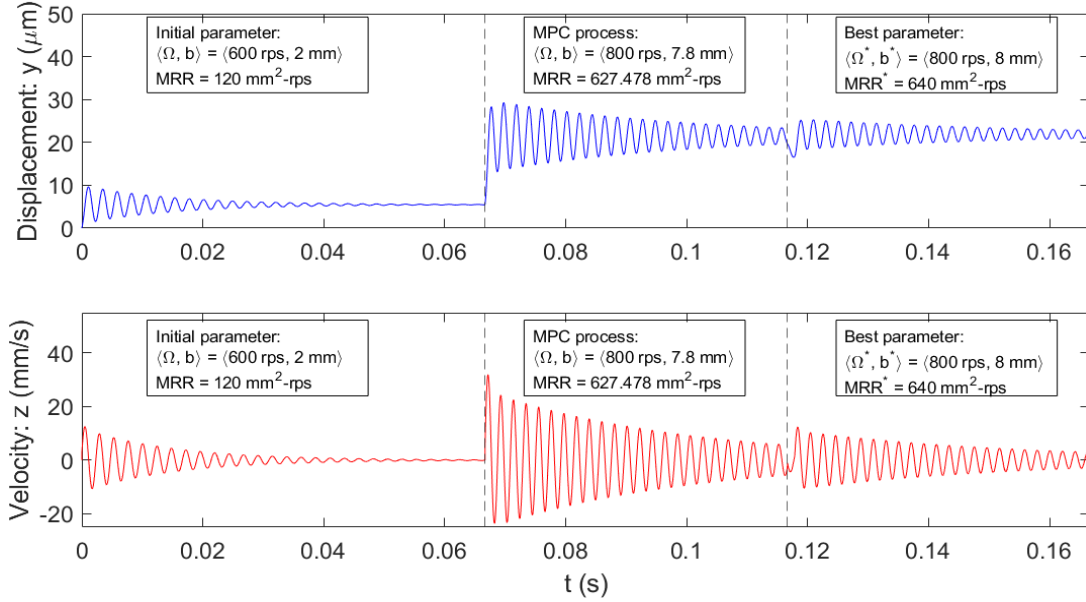


Fig. 6. The trajectories of displacement in (a) and velocity in (b) during the MPC process. The best cutting parameter $\langle \Omega^*, b^* \rangle = \langle 800, 8 \rangle$ is found in the second iteration of MPC.

We report results from the model acquired on data with 10% noise (grey cell in Table 6) for MPC. Fig. 5 shows the results of starting from an initial cut $\langle \Omega_0, b_0 \rangle = \langle 600, 2 \rangle$ (green diamond) and ending at the best cut $\langle \Omega^*, b^* \rangle = \langle 800, 8 \rangle$ (red asterik). The optimal control formulation (24) is solved for three iterations within 3.76 seconds, and the best cut is found in the second iteration of MPC. Note that the stability lobes (magenta curves) are plotted as a reference of the stability boundary. They are not used

during the solution procedure for the optimal control problem. Fig. 6 depicts the time series trajectory of displacement and velocity under the identified parameters during the MPC process. The magnitude decrease of these state variables over time validates the stability for the identified cutting parameters. The initialized cutting parameter with MRR of $120 \text{ mm}^2\text{-rps}$ is improved to the best cutting parameter setting with MRR of $640 \text{ mm}^2\text{-rps}$. This change is evidence for the effectiveness and efficiency of the optimal control formulation (24) in identifying the best cutting parameters.

In summary, the anti-noise capability of PIMLC is at least 100 times better than SINDY-MPC for system identification of turning machine tool using sim-to-real data. The proposed PIMLC can be used for pre-process selection of stable cutting parameters with maximized material removal rate within seconds. This shows that the PIMLC method has the potential to be used for both system identification and pre-process cutting parameter selection in real time of practical turning machine tool operations.

5. Conclusions

This paper presents a data-driven modeling and control effort for nonlinear dynamic systems with highly noisy measurements. A physics-informed machine learning-based control method, denoted as PIMLC, is proposed to acquire white-box models from highly noisy data and integrate the acquired models as physical models into model predictive control framework for control applications. PIMLC extends current discrete optimization-based physics-informed machine learning capabilities to model nonlinear dynamic systems with control. The adoption of such physics-informed machine learning capabilities for PIMLC yields powerful performance for robust system identification despite highly noisy measurements. Benefiting from the accuracy and robustness of acquired white-box models, subsequent model predictive control procedure exhibits superior control performance. Simulation experiments on the chaotic Lorenz 3 system and turning machine tool are conducted with comparisons of PIMLC to the state-of-the-art SINDY-MPC and NARX-MPC methods. The proposed method outperforms SINDY-MPC and NARX-MPC in both model accuracy and control performance under high noise conditions. Furthermore, PIMLC is shown to identify stable cutting parameters with a maximized material removal rate for turning machine tool

operations. Future work will focus on extending the proposed method to milling machine tools for chatter suppression in practice, and designing advanced machine learning methods for data-driven modeling and control of nonlinear dynamic systems when the systems cannot be symbolically representable.

Acknowledgement

The authors acknowledge support from the NSF Engineering Research Center for Hybrid Autonomous Manufacturing Moving from Evolution to Revolution (ERC-HAMMER) under Award Number EEC-2133630. This work was partially supported by the DOE Office of Energy Efficiency and Renewable Energy (EERE), under contract DE-AC05 00OR22725. The US government retains and the publisher, by accepting the article for publication, acknowledges that the US government retains a nonexclusive, paid-up, irrevocable, worldwide license to publish or reproduce the published form of this manuscript, or allow others to do so, for US government purposes. DOE will provide public access to these results of federally sponsored research in accordance with the DOE Public Access Plan (<http://energy.gov/downloads/doe-public-access-plan>). The authors also acknowledge the seed funding from the AI TENNessee Initiative to partially support this research.

References

- [1] Bryson, A.E. and Y.-C. Ho, *Applied optimal control: optimization, estimation and control*. 1975: CRC Press.
- [2] Garcia, C.E., D.M. Prett, and M. Morari, *Model predictive control: Theory and practice—A survey*. Automatica, 1989. **25**(3): pp. 335-348.
- [3] Soudbakhsh, D., A.M. Annaswamy, Y. Wang, S.L. Brunton, J. Gaudio, H. Hussain, D. Vrabie, J. Drgona, and D. Filev. *Data-Driven Control: Theory and Applications*. in *Proceedings of 2023 American Control Conference*. 2023. pp. 1922-1939.
- [4] Akaike, H., *Fitting autoregressive models for prediction*, in *Selected Papers of Hirotugu Akaike*. 1969, Springer. p. 131-135.
- [5] Noriega, J.R. and H. Wang, *A direct adaptive neural-network control for unknown nonlinear systems and its application*. IEEE Transactions on Neural Networks, 1998. **9**(1): pp. 27-34.
- [6] Ho, B. and R.E. Kálmán, *Effective construction of linear state-variable models from input/output functions: Die Konstruktion von linearen Modeilen in der Darstellung durch Zustandsvariable aus den Beziehungen für Ein-und Ausgangsgrößen*. at-Automatisierungstechnik, 1966. **14**(1-12): pp. 545-548.
- [7] Juang, J.-N. and R.S. Pappa, *Effects of noise on modal parameters identified by the eigensystem realization algorithm*. Journal of Guidance, Control, and Dynamics, 1986. **9**(3): pp. 294-303.
- [8] Akaike, H., *A new look at the statistical model identification*. IEEE Transactions on Automatic Control, 1974. **19**(6): pp. 716-723.
- [9] Schmid, P.J., *Dynamic mode decomposition of numerical and experimental data*. Journal of Fluid Mechanics, 2010. **656**: pp. 5-28.
- [10] Chen, K.K., J.H. Tu, and C.W. Rowley, *Variants of dynamic mode decomposition: boundary condition, Koopman, and Fourier analyses*. Journal of Nonlinear Science, 2012. **22**: pp. 887-915.
- [11] Budišić, M., R. Mohr, and I. Mezić, *Applied koopmanism*. Chaos: An Interdisciplinary Journal of Nonlinear Science, 2012. **22**(4).
- [12] Mezić, I., *Spectral properties of dynamical systems, model reduction and decompositions*. Nonlinear Dynamics, 2005. **41**: pp. 309-325.
- [13] Rowley, C.W., I. Mezić, S. Bagheri, P. Schlatter, and D.S. Henningson, *Spectral analysis of nonlinear flows*. Journal of Fluid Mechanics, 2009. **641**: pp. 115-127.
- [14] Kocijan, J., R. Murray-Smith, C.E. Rasmussen, and A. Girard. *Gaussian process model based predictive control*. in *Proceedings of the 2004 American Control Conference*. 2004. pp. 2214-2219.
- [15] Asadi, F., A. Olleak, J. Yi, and Y. Guo. *Gaussian process (gp)-based learning control of selective laser melting process*. in *Proceedings of the 2021 American Control Conference*. 2021. pp. 508-513.
- [16] Han, F. and J. Yi, *Stable learning-based tracking control of underactuated balance robots*. IEEE Robotics and Automation Letters, 2021. **6**(2): pp. 1543-1550.
- [17] Chen, K., J. Yi, and D. Song, *Gaussian-Process-Based Control of Underactuated Balance Robots With Guaranteed Performance*. IEEE Transactions on Robotics, 2022. **39**(1): pp. 572-589.

- [18] Yi, J., Y. Sheng, and C.S. Xu, *Neural network based uniformity profile control of linear chemical-mechanical planarization*. IEEE Transactions on Semiconductor Manufacturing, 2003. **16**(4): pp. 609-620.
- [19] Yin, Z., T. Liu, C. Wang, H. Wang, and Z.-P. Jiang, *Reducing urban traffic congestion using deep learning and model predictive control*. IEEE Transactions on Neural Networks and Learning Systems, 2023: pp. 4131-4145.
- [20] Kaiser, E., J.N. Kutz, and S.L. Brunton, *Sparse identification of nonlinear dynamics for model predictive control in the low-data limit*. Proceedings of the Royal Society A, 2018. **474**(2219): pp. 20180335.
- [21] Shi, Z., H. Ma, H. Tran, and G. Zhang, *Compressive-sensing-assisted mixed integer optimization for dynamical system discovery with highly noisy data*. arXiv preprint arXiv:2209.12663, 2022.
- [22] Bertsimas, D. and W. Gurnee, *Learning sparse nonlinear dynamics via mixed-integer optimization*. Nonlinear Dynamics, 2023. **111**(7): pp. 6585-6604.
- [23] Brunton, S.L., J.L. Proctor, and J.N. Kutz, *Discovering governing equations from data by sparse identification of nonlinear dynamical systems*. Proceedings of the National Academy of Sciences, 2016. **113**(15): pp. 3932-3937.
- [24] Mangan, N.M., T. Askham, S.L. Brunton, J.N. Kutz, and J.L. Proctor, *Model selection for hybrid dynamical systems via sparse regression*. Proceedings of the Royal Society A, 2019. **475**(2223): pp. 20180534.
- [25] Wang, W.-X., R. Yang, Y.-C. Lai, V. Kovanis, and C. Grebogi, *Predicting catastrophes in nonlinear dynamical systems by compressive sensing*. Physical Review Letters, 2011. **106**(15): pp. 154101.
- [26] Drgoňa, J., K. Kiš, A. Tuor, D. Vrabie, and M. Klaučo, *Differentiable predictive control: Deep learning alternative to explicit model predictive control for unknown nonlinear systems*. Journal of Process Control, 2022. **116**: pp. 80-92.
- [27] Schmitz, T.L. and K.S. Smith, *Machining dynamics*. Springer, 2009: pp. 303.
- [28] Tyler, C.T., J.R. Troutman, and T.L. Schmitz, *A coupled dynamics, multiple degree of freedom process damping model, Part 1: Turning*. Precision Engineering, 2016. **46**: pp. 65-72.
- [29] Salehi, M., T. Schmitz, R. Copenhaver, R. Haas, and J. Ovtcharova, *Probabilistic sequential prediction of cutting force using Kienzle model in orthogonal turning process*. Journal of Manufacturing Science and Engineering, 2019. **141**(1): pp. 011009.